Intelligent Service Robotics (2022) 15:661–669
https://doi.org/10.1007/s11370-022-00443-5

ORIGINAL RESEARCH PAPER

Experimental investigation of a new type of driving concept for capsule robot

Linlin Wu[1] · **Kaiyuan Lu**[2]

Received: 30 November 2021 / Accepted: 22 August 2022 / Published online: 27 September 2022

Abstract
Although the physical examination using conventional capsule endoscopy can be achieved in a non-invasive and painless way, it is a costly, long-time and uncontrollable procedure. The active driving mechanism for capsule endoscopes is thus proposed on the basis of the conventional capsule endoscope. This paper studies a new actuator structure for potential active capsule robot (CR) applications. This actuator, which consists of a single inner mass and an outer smooth shell, is designed to be able to realize a sealed linear locomotion system, avoiding damaging the intestinal tissue caused by the paddle or leg sticking outside the capsule that are often shown in other CR designs. Compared to the existing driving principle, the CR proposed in this paper is driven by the collision impact forces generated inside the capsule, rather than by additional mechanical structures of the CR or micro-motors within the capsule to generate the required driving force. When the excited current in the coil is 2.75 amps, the driving force acting on the capsule body is approximately 2 N, which is larger than other existing conventional actuators. Moreover, the measured experimental results show that the stroke length and movement speed can be easily controlled by varying the amplitude and frequency of the excitation current purely.

Keywords Capsule robot · Permanent magnet · Collision force · Capsule locomotion

1 Introduction

Capsule endoscopy (CE) as a promising alternative endoscopic enables to visualize and detect the whole gastrointestinal (GI) tract, especially for the small intestine area [1–5]. The capsule robots that have been proposed are either active or passive, depending on whether they have an active drive mechanism. Although the passive CRs have been successfully used in clinical applications, they have the defects of missed inspection or unable to check the lesion area repeatedly [6, 7]. In recent years, a type of wireless CR has attracted great attentions of the academic researchers in various fields [8–14]. However, the existing locomotion system is still a key limitation for the capsule products, since the current commercial CEs could travel through the human body in a passive way only [15, 16]. Moreover, the lack of controlled locomotion of the existing CEs has been an obstacle for extending its practical applications [17]. An active locomotion system is therefore desired to achieve, e. g., forward or backward movement for meeting real-time control demands required by more advanced clinical applications [18, 19]. The active capsule robot has the characteristics of controlled travel direction, position and speed, helping to improve the efficiency of diagnosis and treatment effectively. These motivate the research and development on the active capsule endoscope, which is also called capsule robot or CR.

To achieve an active CR, generally speaking, three more sub-systems are often implemented on the CR side: the actuator mechanism, the attached mechanical system, and the bionic locomotion mechanism [17, 20]. The different adoptions of these alternatives have been formed of various different locomotion mechanisms as well as its working principles [20]. For instance, some CRs can be driven by the micro-actuator with external driving mechanism, e. g., legs, pedals or needles, interacting with the non-smooth surface of the organ wall [21–23], while the other types are driven by the external magnetic (electromagnetic) field interacting with the permanent magnet embedded inside CR [24–26]. However, the use of the external legs or pedals has the risk of intestinal tissue damage; manipulating the CR by external magnetic field will require strong magnetic field sources

✉ Linlin Wu
LLWu_et_1105@126.com

[1] Shanghai Dianji University, Shanghai, China

[2] Aalborg University, 9220 Aalborg, Denmark

since the magnetic field decreases dramatically when the distance increases.

Currently, a two-mass-based locomotion system as a promising technology has been well reported and studied in [27–32]. This locomotion system consists of an internal mass and an outer rigid encapsulated body, and this makes it easier to be miniaturized and completely sealed. The working principle is that the whole system can be propelled rectilinearly by the internal interaction force created by the internal mass when excited by a periodic force [28, 31]. So far, it has been proposed for the engineering, medical, and disaster fields [33]. Due to the structure advantage of forming a sealed and rigid body without external legs or pedals, this locomotion mechanism is suitable to be applied in a restrict space such as the intestinal tract [34, 35]. A vibro-impact-based locomotion system consisting of two moving inner masses was proposed to be applied for the active CR by Cherousko [36]. Later, to optimize the system parameters to meet the medical application demands, a vibro-impact-based CR consisting of a capsule body and an internal mass driven by a harmonic excitation was presented in [35, 37, 38]. Dynamic behavior and simulation model of the vibro-impact-based CR system are both studied in detail in [31–34, 39]. Moreover, a detailed investigation on the capsule motion profiles under various external friction forces has been carried out in [40]. However, for those aforementioned actuator systems, they are restricted by the limited driving force, complicate structure, or the uncontrolled elastic vibration. In these proposed structures, a spring is normally used to connect the internal mass and the encapsulated body, as an important part of its mechanical, leading to a potentially weakened system reliability.

In this paper, a new simple active actuator applied for CR is proposed. The main feature of this new structure is the large driving force produced by the collision action between the internal mass and the CR. The detailed structure and the working principle of this new CR are explained in Sect. 2. In Sect. 3, the analysis of its locomotion characteristic is provided. The experimental results measured on the CR prototype are presented in Sect. 4. Section 5 concludes this paper.

2 The proposed new CR

2.1 Capsule robot structure

The new CR proposed in this paper consists of three cylindrical permanent magnets (PMs) and one small solenoidal coil as principally illustrated in Fig. 1a. A corresponding CR prototype was manufactured and is shown in Fig. 1b. Two of the PMs, namely PM1 and PM2, are attached to the two ends of the capsule body, while the PM3 is attached to the small coil in between the capsules. PM1 and PM2 face each other with the same polarity, while PM3 and PM2, separated by the small coil, face each other with opposite polarities. In addition, a small reflecting plate is mounted to one side of the coil bobbin in the prototype CR, which is used to measure the displacement of the small coil by a laser sensor.

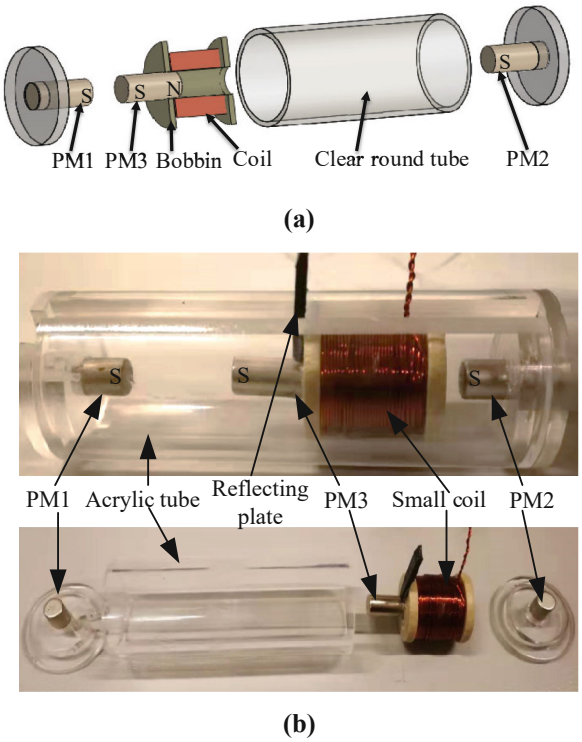

Fig. 1 Structure of the new CR prototype: **a** explosion structure of the CR, **b** the proposed CR prototype

This new CR has a simple structure. It can realize a controlled linear locomotion, by adjusting the amplitude or frequency of the current supplied to the small coil. The working principle of the CR is explained in detail as below.

2.2 The CR working principle

The schematic diagram of the proposed CR is shown in Fig. 2. Pulsed current is supplied to the small coil to drive the CR move forward. The locomotion of this CR in one cycle may be divided into three stages, as discussed below.

- Stage 1, when the supplied current is zero, both the internal small coil and the rigid capsule body will remain standstill, parked at an initial position as shown in Fig. 2a. Due to the attractive force f_{pm} between PM2 and PM3, the coil will be parked next to PM2.
- Stage 2, a pulsed current is supplied to the small coil. This current direction is in such a way that the magnetic field produced by the current will produce repulsive force between the small coil and PM2, and attractive force

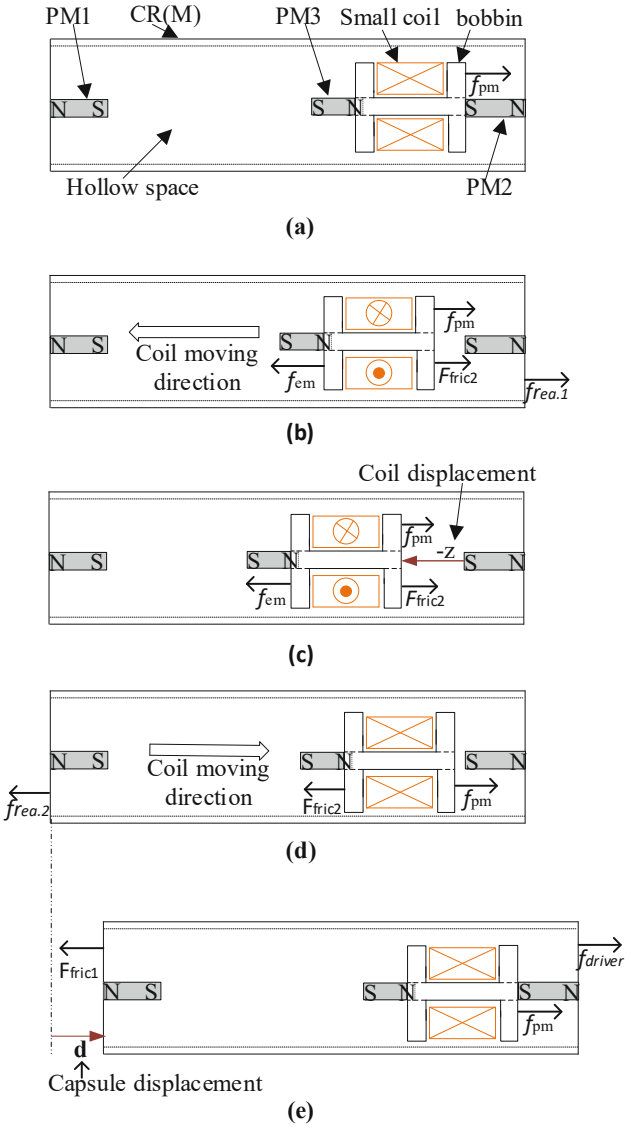

Fig. 2 Stages of the CR locomotion in one cycle: **a** initial state of the capsule robot, **b** the coil begins to move away from PM2 when it is supplied a current, **c** the coil parks at a new position, **d** the coil moves back to PM2, **e** capsule is driven to move forward after collision

between the small coil and PM1. These forces can afford to overcome the frictional force (F_{ric2}) and the magnet attractive force $\left(f_{\text{pm}}\right)$ and drive the small coil to move away from PM2, as illustrated in Fig. 2b. Here, $f_{\text{rea.1}}$ is the corresponding reaction force acting on the CR body. Holding the current to be constant, the small coil thus parks at a new position as shown in Fig. 2c after experiencing a transient period of acceleration and deceleration.

- Stage 3, upon suddenly stopping the current supplied to the small coil, the repulsive (/attractive) force between PM1 (/PM2) and PM3 attached to the small coil will then drive the small coil and PM3 back to its original position (Fig. 2d). During this period, a counter direction reactive force $f_{rea.2}$ acting on CR body will be generated, and the small coil will continue to be accelerated until it hits the end magnet PM2. The collision behavior between the small coil and the PM2, according to the conservation of momentum principle, will generate a large collision force acting on the external capsule, and it affords to drive the CR to move forward, as illustrated in Fig. 2e. Repeating this pulsed current supplied to the small coil, stepwise locomotion of the CR can then be achieved.

It is important to point out that when the current suddenly reduces to zero, the coil will begin to accelerate toward PM2 due to the attractive force between PM3 and PM2. This kind of acceleration can generate a counter direction reactive force on the capsule body. This is the fundamental driving principle of many existing internal vibration-driven-based locomotion systems. Depending on the acceleration, this reactive force may not be large enough to move the capsule body. But by utilizing the collision action between the small coil and the capsule body, the coil behaviors like a 'hammer' quickly punch the capsule. Therefore, large driving force will be produced and the CR can be driven forward. This is the new driving concept proposed in this paper and allows producing a large force for driving the CR.

3 Modeling and analysis

3.1 Finite element modeling (FEM) results

A 3D schematic model built in COMSOL is shown in Fig. 3a, and its geometric parameters are given in Table 1. A view on the cross-sectional plane showing the flux density and flux lines is given in Fig. 3b. The plotted flux density shown in Fig. 3b is achieved under the condition of a DC current supplied to the small coil at the initial parking position Z = 0. This position is shown in Fig. 2a as well as Fig. 3a. To drive the small coil to move toward PM1, the driving force, existing between the two end PMs (PM1 and PM2) and the small coil with a current, should be on the -z-axis as indicated in Fig. 3a. Different force profiles acting on the small coil with different coil DC currents at different locations of the small coil are obtained by FEM. The results are shown in Fig. 4a.

As may be observed from Fig. 4a, at the initial parking position ($Z = 0$ mm) and zero coil current, the force acting on the coil is positive, meaning it is pointing at PM2 (the attractive force between PM3 and PM2). If a positive DC current is supplied to the coil, the force will become negative and drive the coil to move away from PM2, towards PM1. As the distance between the coil and PM2 increases, the coil current-related force component becomes less influential on the total force.

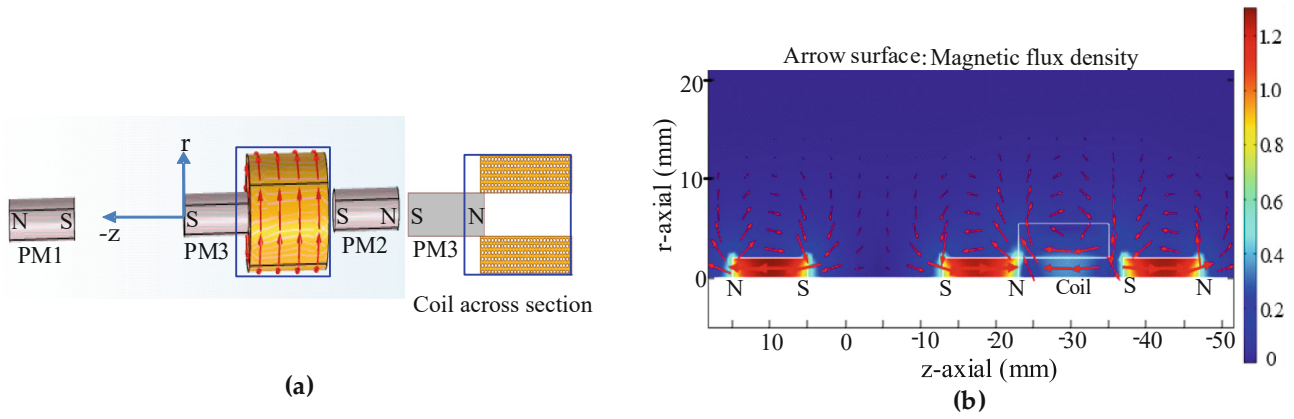

Fig. 3 The FE model simulated by Comsol: **a** 3D model of the CR prototype, **b** 2D plot of the magnetic flux density distributions and flux lines

Table 1 Finite element model-related parameters according to the capsule prototype

Parameter	Value	Unit
Coil inner radius	2	mm
Coil thickness	3.5	mm
Coil length	12	mm
Magnet radius	2.5	mm
Magnet length	10	mm
Magnet remanence	1.074	T
Iron mass	0.362	g
Iron diameter	3	mm
Iron height	12	mm
Inner mass (m)	10.32	g
Total capsule mass (M)	28.15	g
Friction coefficient ($\mu 1$)	0.2	
Capsule length	60	mm
Capsule inner diameter	12	mm
Capsule outer diameter	14	mm

In practice, the supplied current is a pulsed current as shown in Fig. 4b (the blue curve). The corresponding force profile (light green line) obtained at different coil positions (red line) in one cycle is also given in Fig. 4b. It can be observed that in the $t1$ period, since there is no current, the force exerted on the coil is constant, locking the coil at its initial parking position (corresponding to Fig. 2a). In the beginning of the $t2$ period, a pulsed current as shown in Fig. 4b is supplied to the small coil, and then, the force will change to negative and drive the coil to move away from PM2 (corresponding to Fig. 2b). As the distance between the coil and PM2 increases, the force between the two end PMs and the internal moving mass will decrease and eventually becomes positive. In the $t3$ period, a new parking position is achieved (corresponding to Fig. 2c). In the period of $t4$, the coil current is removed and the positive attractive force between PM3 and PM2 will drive the coil to move toward PM2 (corresponding to Fig. 2d). In this period, the coil is kept being accelerated until it hits PM2. Eventually in the

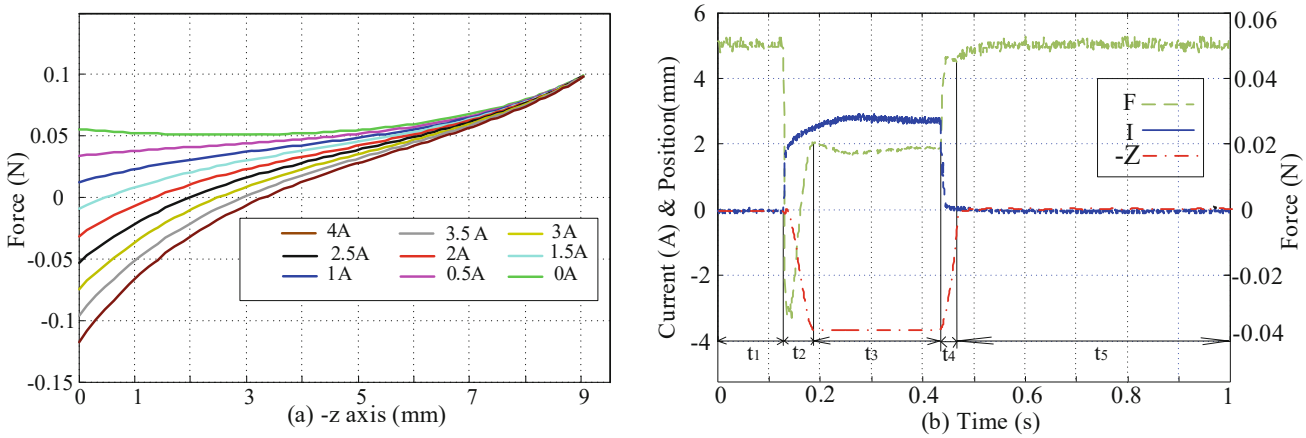

Fig. 4 The simulation results achieved by the FE method: **a** the force profiles acting on the small coil with different DC currents and displacements of the coil with respect to PM2, **b** the force profile acting on the small coil under pulsed current excitation in one cycle

$t5$ period, the coil will touch PM2 and park at its original position. The force exerted on this coil will also reach its maximum value of around 0.055 N. This completes a driving cycle of this CR.

3.2 Mathematical modeling

As explained in Sect. 2, both the CR and small coil motions depend on the supplied current in the small coil, while the displacement of the small coil with respect to PM2 has a direct effect on the collision force, which is the driving force of the proposed CR. To simplify the modeling, both stage 1 and stage 2 are ignored and only stage 3 is considered. At the beginning of stage 3, since the current in the small coil is suddenly reduced to zero, the forces including the attractive force between PM3 and PM2 and the repulsive force between PM3 and PM1 will together act on the inner mass and drive it to move backwards to its original position. These two magnetic forces will change when the distance between PM2 and PM3 reduces. Furthermore, in this process, the useful work will be converted into the kinetic energy of the inner mass which will be released when the coil hitting PM2 at a large velocity. This procedure can be described as:

$$\int_{-z}^{0} \left(f_{\mathrm{pm}}(z) - F_{\mathrm{fric2}}\right)\mathrm{d}z = \frac{1}{2}m\dot{z}^2 \tag{1}$$

where f_{pm} is the magnetic force acting on small coil due to the interaction between PM3 and PM1, and PM3 and PM2, when the current in the coil is zero; m is the mass of the inner moving part including the small coil and PM3; -z is used to indicate the displacement of the small coil as illustrated in Fig. 2c; F_{fric2} is the friction force between the inner mass and the inner surface of the capsule.

To describe the collision, the principle of conservation of momentum is used. Before collision, the coil has a velocity, while the capsule remains at standstill. After collision, the coil and the capsule move together as a rigid body. Therefore, it can be obtained that

$$m\dot{z} + 0 = M\dot{d} \tag{2}$$

where M is the total mass of the CR prototype and d is the capsule displacement, as indicated in Fig. 2e.

After the collision action, the CR will begin to move forward because of the large collision force acting on capsule body. The stored energy in the accelerated coil has to be released, overcoming the frictional force acting on the capsule when it moves. This suggests that:

$$\frac{1}{2}M\dot{d}^2 = F_{fric1}d \tag{3}$$

$$f_{\mathrm{driver}} - F_{\mathrm{fric1}} = M\ddot{d} \tag{4}$$

The external frictional force (F_{fric1}) between the capsule and its contact surface is determined by the friction coefficient and the total capsule weight, as:

$$F_{\mathrm{fric1}} = \mathrm{sgn}(\dot{d})\mu_1 Mg \tag{5}$$

where F_{fric1} is the friction force between the capsule and the contact surface, μ_1 is the coefficient friction, $g = 9.8\ \mathrm{m/s^2}$ as the gravity acceleration constant and f_{driver} is the collision force acting on the CR.

Combining (1), (2), (3), (4) with (5), we have

$$d = \frac{m * \int_{-z}^{0} \left(f_{\mathrm{pm}}(z) - F_{\mathrm{fric2}}\right)\mathrm{d}z}{\mu_1 * M^2 * g} \tag{6}$$

This equation shows that the capsule displacement is proportional to the coil mass while inversely proportional to the total mass squared. For the same masses, a larger magnetic force f_{pm} will lead to a larger capsule displacement. The magnetic force f_{pm} depends on the displacement between the coil and PM2 (Fig. 2c).

4 Experiment results

4.1 Experiment setup

An experimental platform to validate the new driving concept of the CR system is built as shown in Fig. 5. It consists of two parts: the locomotion unit and the measurement unit. The locomotion unit includes an acrylic guiding slot and a capsule prototype, while the measurement unit is one ILD 1420 laser sensor. Its displacement measurement accuracy can reach 1 μm.

According to the working principle of the CR described above, the capsule prototype will perform the linear motion on this platform when a pulsed current is supplied to the small

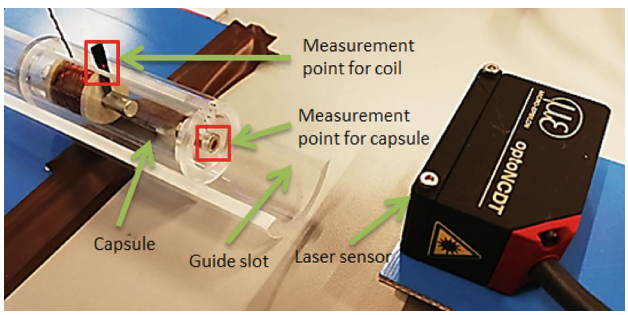

Fig. 5 Experimental test bench

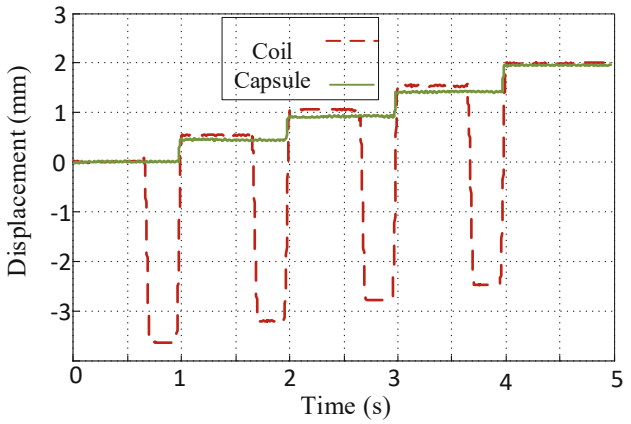

Fig. 6 Displacement profiles of the linear actuator and capsule

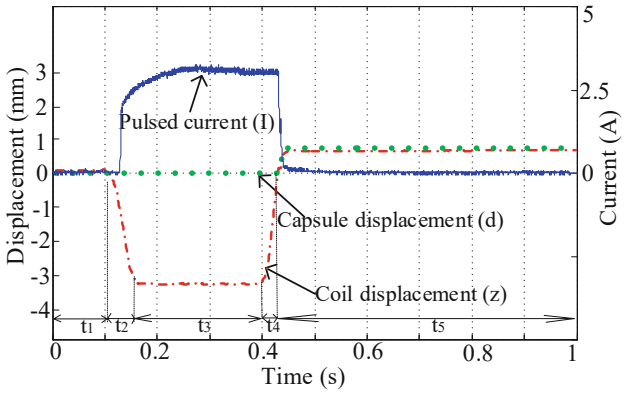

Fig. 7 Enlarged view of the measured current and displacement profiles in one period

coil. To further analyze the CR motion, the displacements of both the small coil and the capsule were recorded. The two displacement measurement points aimed by the laser are indicated in Fig. 5. As an example of current cycle, the pulsed current has an amplitude of 2.75A, a frequency of 1 Hz, as well as a duty ratio of 0.3. The resultant displacement profiles of the coil and the CR are shown in Fig. 6, respectively. It can be clearly observed from Fig. 6 that the coil has a large negative (moving away from PM2) displacement at first and then back to its original position. Upon hitting PM2, the coil and the capsule will move forward together. In addition, a clear stepwise forward moving profile of the capsule can also be observed from Fig. 6. An enlarged view of the displacement profiles for the coil and the capsule, and a supplied current waveform are given in Fig. 7. Following the similar analysis to the profile given in Fig. 4b, in the $t1$ period, there is no current and the coil parks at its original position. When the current increases in period $t2$, the displacement of the coil is negative (moving away from PM2) and will stay at a new position as explained before. When the current reduces to zero in period 3, the coil moves back to its original position and then moves forward together with the capsule. Repetitive oscillation of the small coil under a pulsed current will result in a discontinuous stepped locomotion of the CR as illustrated in Fig. 6. The measured experimental results in Fig. 6 confirm that this new collision-driven-based locomotion design idea is a feasible solution and it also opens a new possibility for realizing linear movement.

4.2 Analysis of the enhanced driving force mechanism

It is claimed before that much larger force will be generated when the coil collides with the capsule body than that produced during coil the acceleration period. This phenomenon will be analyzed here. As may be observed from Fig. 7, in the beginning of the $t4$ period, the coil accelerates back to its original position. The acceleration is generated by the attractive force between PM3 and PM2. A counter acceleration force will be applied on the capsule body in this period. The experiment result has indicated that during this acceleration period, the capsule body remains standstill. The counter reaction force on the capsule body is not large enough to overcome the frictional force between the capsule and the guiding slot. However, when the coil moves back to its original position, colliding with the capsule body, both the coil and capsule can move forward together. This implies that during the collision, much larger force is generated which is now able to overcome the frictional force and drive the capsule to move forward.

According to the law of momentum conservation, ideally, the total momentum of the two-mass system before and after the collision should be the same, as described by (2). Therefore, to illustrate this principle, the system momentum is calculated before and after the collision using the measured displacement, velocity and acceleration. Before the collision, the system momentum is the momentum of the coil (which is $m\dot{z}$) since the capsule remains standstill. By observing the coil velocity before collision given in Fig. 8 and using the coil mass given in Table 1, taking the measurements for the first cycle as an example, the momentum of the coil before collision is found to be 1.65 g·m/s. After collision, the CR together with the small coil will begin to move forward together. Only the frictional force between the capsule body and the guiding surface will be applied on the capsule for deceleration. By observing the peak velocity achieved after collision and using the total mass of the coil and the capsule, the system momentum after collision $\left(M\dot{d}\right)$ can then be obtained. Taking the first cycle as an example, the momentum is found to be around 1.69 g·m/s. It is close to the momentum obtained before the collision observed in the same cycle. The momentum after collision should not be larger than the momentum before the collision. The difference observed from the experiment is due to measurement errors. The experiment was repeated for 4 cycles, and it can

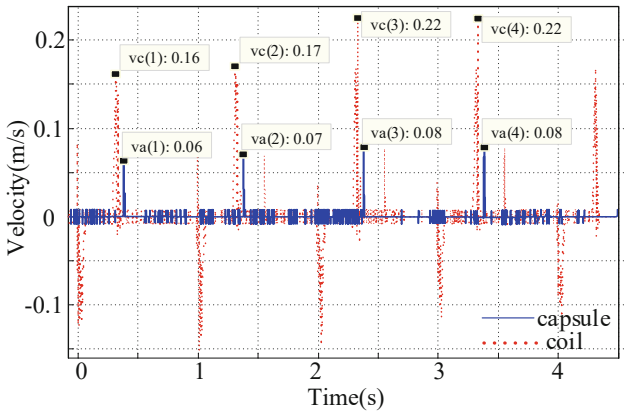

Fig. 8 The recorded four periods for the velocities of the small coil and the CR

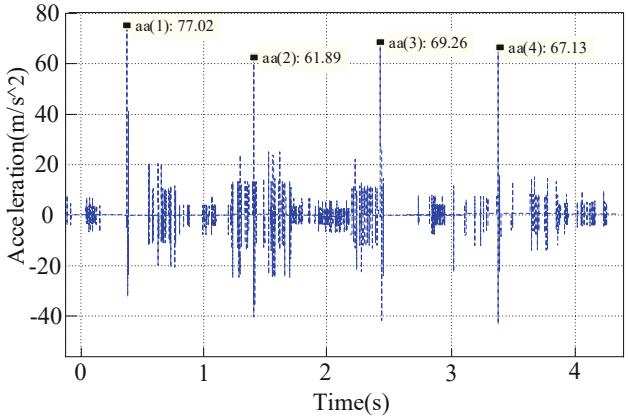

Fig. 9 The recorded four periods for the accelerator of the CR

be observed from Fig. 8 that the observed speed varies a bit. This is possibly due to manufacturing tolerances of the coil bobbin since coil may not move perfectly in parallel with the capsule inner surface, and possible variation of the frictional force as well, etc. Observed from Fig. 8, for the remaining three cycles, the obtained momentums before collision are found to be 1.75 g m/s, 2.27 g m/s, and 2.27 g m/s, respectively. After the collision, the momentums are 1.97 g m/s, 2.25 g m/s and 2.25 g m/s, respectively.

Before collision, the reaction force acting on the CR is equal to the resultant force acting on the small coil used for acceleration. If the frictional force is neglected, then this maximum available force for acceleration will be the maximum attractive force between PM3 and PM2. According to the force profiles given in Fig. 4b, the maximum resultant force acting on the small coil is achieved at its original position when the current is zero. Thus, the maximum reaction force acting on the CR before collision can reach about 0.055 N. After collision, the reaction force acting on the capsule can be calculated by (4), which is the total mass of the coil and capsule multiplying the acceleration. The acceleration of the CR for the capsule in four periods is given in Fig. 9. It indicates obviously that the maximum acceleration in one cycle is achieved only at the collision moment. Therefore, the collision force in four periods could be calculated, which are 2.2 N, 1.7 N, 1.9 N, and 1.9 N, respectively.

Comparing the reaction force acting on the capsule body before collision with the one after the collision, the collision action can generate much higher driving force on the capsule, nearly 35 times in average. The results indicate that this new active actuator, which is designed according to the collision principle, can generate much larger driving force than other existing conventional actuators.

4.3 Controllability analysis

As it is described in Sect. 3, the CR displacement is mainly determined by the supplied current in the small coil. This pulsed current has three key factors, i.e., the current amplitude, frequency and the current duty ratio. In order to evaluate their effects on the CR displacement, the experimental results of the capsule displacement under different currents are measured by laser sensor as shown in Figs. 10, 11 and 12, respectively.

In Fig. 10, these CR displacement curves are measured with different amplitudes of the supplied current, e.g., 2.25 A and 2.75 A, a constant frequency of 1 Hz and a fixed duty ratio of 0.3. This figure indicates that the measured CR displacement increases when with the increased amplitude of the supplied current. This is because as the current increases, the coil can be driven further away from PM2, resulting in a longer distance for acceleration toward PM2 and larger momentum.

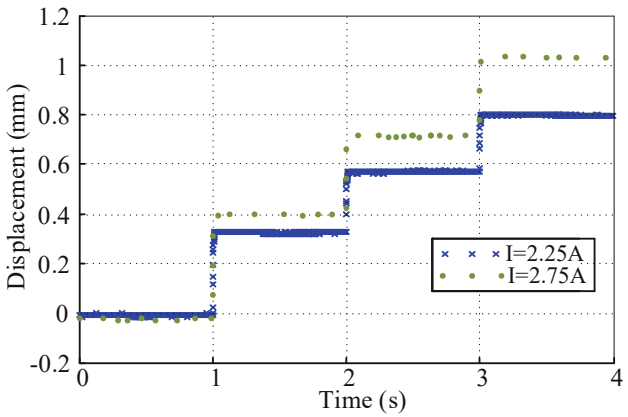

Fig. 10 The measured displacements of the capsule VS. current amplitude

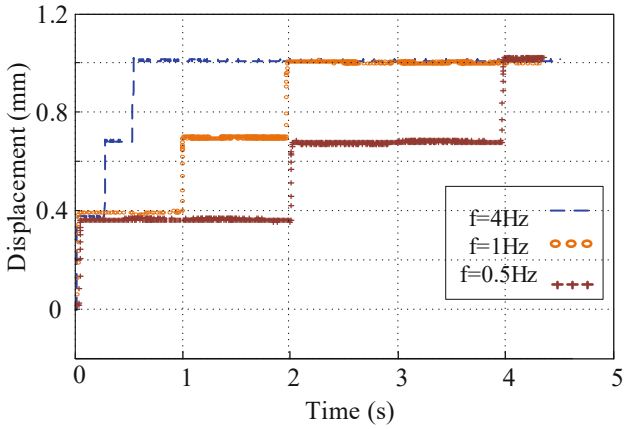

Fig. 11 The measured displacements of the capsule VS. current frequency

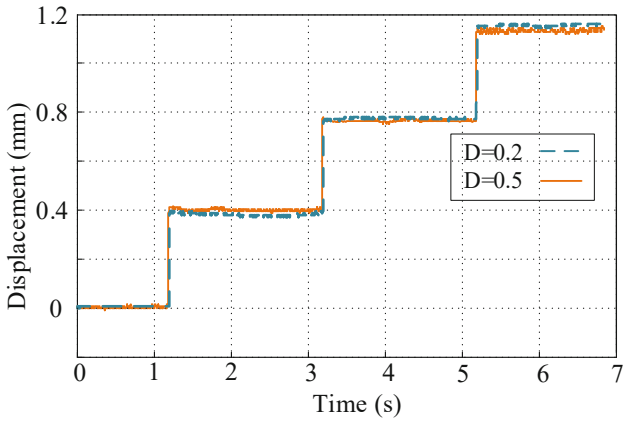

Fig. 12 The measured displacements of the capsule VS. current duty

In Fig. 11, the CR displacements in 2 periods are measured with varying current frequencies, which are 0.5 Hz, 1 Hz and 4 Hz, respectively. The current amplitude is kept constant to be 2.75 A, and the duty ratio is fixed to 0.3. These curves demonstrate that the current frequency has a great impact on the CR displacement speed. As the frequency of the supplied current increases, the time needed for completing a locomotion cycle reaching the same displacement will be shortened. In other words, the moving velocity of the capsule is increased. This is a simple approach to control the capsule velocity. The independent effects of the current amplitude and frequency on the moving profile of the capsule improve the controllability of the capsule.

The displacements of capsule in 3 periods measured with different duty ratios of the pulsed current are shown in Fig. 12. The frequency of the pulsed current is fixed to 1 Hz, and the current amplitude is maintained at 2.75 A. The experimental results reveal that the current duty ratio has negligible effects on the capsule displacement. The force available for driving the capsule is mainly determined by the parking distance between the coil and PM2 (e.g., Figure 2c) for a given current.

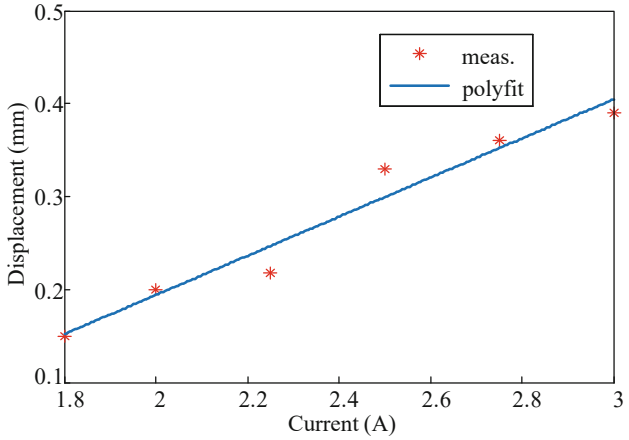

Fig. 13 Measured capsule displacement (d) VS. current amplitude

How long the coil parks there, which is determined by the duty ratio, will not matter.

The profile of the capsule displacement vs. supplied current amplitude is given in Fig. 13. The capsule displacements were recorded for 10 continuous periods and then averaged. The measurement was repeated for different current amplitudes. It may be observed from Fig. 13 that the capsule displacement is proportional to the current amplitude. This linear relationship is preferred since it will simplify a control system design for such a linear CR.

5 Conclusion

This paper proposed a sealed actuator mechanism for potential active in vivo capsule applications. The feasibility of the new CR and its driving concept are confirmed experimentally in the laboratory on a prototype, with detailed analyses provided. The experimental results have demonstrated that the capsule locomotion is mainly affected by two key factors, namely the amplitude and the frequency of the supplied pulsed current. The experimental results can also be used to optimize the mechanical structure parameters of the capsule prototype, which will help to further miniaturize the experimental prototype of the CR to capsule size in the future.

Compared to the actuator systems based on additional mechanical structures outside or inside the CR to drive the movement of the capsule described in other papers, this paper presents a simpler, easier to control and safer active mechanism. In addition, this actuator mechanism will be used in the future to explore more practical medical functions of the CR, such as positioning, rotation, drug delivery and release, and biopsy. In addition, in future work we will continue to work on completing its integrated circuit system and wireless power transmission system to achieve a more perfect CR system.

Declarations

Conflict of interest The authors have no conflict of interest to disclose.

References

1. Marya S, Jawaid A, Foley S, Han K, Patel L (2019) A randomized controlled trial comparing efficacy of early video capsule endoscopy with standard of care in the approach to nonhematemesis GI bleeding. Gastrointest Endosc 89:33–43
2. Saurin JC, Beneche N, Chambon C et al (2016) Challenges and future of wireless capsule endoscopy. Clinical Endo 49:26–29
3. Hejazi RA, Bashashati M, Saadi M et al (2016) Video capsule endoscopy: a tool for the assessment of small bowel transit time. Front Med 3:5
4. Abbas B, Fatemeh A, Reza A (2020) Integrated system for automatic detection of representative video frames in wireless capsule endoscopy using adaptive sliding window singular value decomposition. IET Image Proc 14:147–153
5. Valdastri SM, Webster RJ (2012) Advanced technologies for gastrointestinal endoscopy. Annu Rev Biomed Eng 14:397–429
6. Quirini M, Menciassi A, Scapellato S, Stefanini C (2018) Design and fabrication of a motor legged capsule for the active exploration of the gastrointestinal tract. IEEE/ASME Trans Mechatron 13:169–179
7. Chun HJ, Tanabe S, Choi MG et al (2016) Current status and future directions of capsule endoscopy. Gastroenterol Res Pract 2016:1–51
8. Zhou H, Alici G, Munoz F (2016) A magnetically actuated anchoring system for a wireless endoscopic capsule. Biomed Microdevices 18:102
9. Caprara R, Obstein KL, Scozzarro G et al (2015) A platform for gastric cancer screening in low-and middle-income countries. IEEE Trans Biomed Eng 62:1324–1332
10. Alshorman A, Hurmuzlu Y (2018) Kinematic locomotion modes of particle-based linear chain mechanisms. ASME J Dyn Sys Meas Control. https://doi.org/10.1115/1.4037735
11. Lee C et al (2015) Active locomotive intestinal capsule endoscope (ALICE) system: A prospective feasibility study. IEEE/ASME Trans Mechatron 20:2067–2074
12. Liu L, Towfighian S, Hila A (2015) A review of locomotion systems for capsule endoscopy. IEEE Rev Biomed Eng 8:138–151
13. Ciuti G, Menciassi A, Dario P (2011) Capsule endoscopy: from current achievements to open challenges. IEEE Rev Biomed Eng 4:59–72
14. Ciuti G, Caliò R, Camboni D, Neri L, Bianchi F, Arezzo A et al (2016) Frontiers of robotic endoscopic capsules: a review. J Micro-Bio Robot 11:1–18
15. Pullens HJ, Van-der-Stap N, Rozeboom ED et al (2016) Colonoscopy with robotic steering and automated lumen centralization: a feasibility study in a colon model. Endoscopy 48:286–290
16. Bianchi F et al (2019) Localization strategies for robotic endoscopic capsules: a review. Expert Rev Med Devices 16:1–23
17. Alshorman AM, Ababneh OA, Abushaker AI, Tamimi EM, Baniyassin OZ (2021) A novel design of a locomotion system for Active capsule endoscopy. In: 7th Int Conf Mechatron Robot Eng (ICMRE), pp. 93–97
18. Joyee EB, Pan Y (2019) A fully three-dimensional printed inchworminspired soft robot with magnetic actuation. Soft Rob 6:1
19. Hoang MC, Lee VH, Kim J et al (2019) Untethered robotic motion and rotating blade mechanism for actively locomotive biopsy capsule endoscope. IEEE Access 7:93364–93374
20. Alshorman A, Hurmuzlu Y (2015) Dynamics and control of particle based chain mechanism. PhD thesis, Southern Methodist University.
21. Xie W, Kothari V, Terry BS (2015) A bio-inspired attachment mechanism for long-term adhesion to the small intestine. Biomed Microdevices 17:68
22. Valdastri P, Webster RJ, Quaglia C, Quirini M, Menciassi A, Dario P (2009) A new mechanism for mesoscale legged locomotion in compliant tubular environments. IEEE Trans Robot 25:1047–1057
23. Gregory A, Micah P, Steven A et al (2020) Novel optimization-based design and surgical evaluation of a treaded robotic capsule colonoscope. IEEE Trans Robotics 36:545–552
24. Ching HL, Hale MF, Mc Alindon ME (2016) Current and future role of magnetically assisted gastric capsule endoscopy in the upper gastrointestinal tract. Ther Adv Gastroenterol 9:313–321
25. Zhang YS, Chi ML, Su ZK et al (2016) Critical coupling magnetic moment of a petal-shaped capsule robot. IEEE Trans Magn 52:5000109
26. Lucarini G, Mura M, Ciuti G et al (2015) Electromagnetic control system for capsule navigation: novel concept for magnetic capsule maneuvering and preliminary study. J Med Biol Eng 35:428–436
27. BöhmV KT, Zeidis I, Zimmermann K (2017) Dynamic analysis of a spherical mobile robot based on a tensegrity structure with two curved compressed members. Arch Appl Mech 87:853–864
28. Fang H-B, Xu J (2012) Controlled motion of a two-module vibration-driven system induced by internal acceleration-controlled masses. Arch Appl Mech 82:461–477
29. Liu P, Yu H, Cang S (2018) Geometric analysis-based trajectory planning and control for under actuated capsule systems with viscoelastic property. Trans Inst Meas Control 40:2416–2427
30. Huda MN, Yu H (2015) Trajectory tracking control of an underactuated capsubot. Auton Robots 39:183–198
31. Liu Y, Wiercigroch M, Pavlovskaia E, Yu H (2013) Modelling of a vibro-impact capsule system. Int J Mech Sci 66(2):11. https://doi.org/10.1016/j.ijmecsci.2012.09.012
32. Chernous'ko FL (2011) Analysis and optimization of the rectilinear motion of a two-body system. J Appl Math Mech 75:493–500
33. Liu Y, Pavlovskaia E, Wiercigroch M (2016) Experimental verification of the vibro-impact capsule model. Nonlinear Dyn 83:1029–1041
34. Liu P, Yu H, Cang S (2018) On the dynamics of a vibro-driven capsule system. Arch Appl Mech 88:2199–2219
35. Bolotnik NN, Figurina TY (2008) Optimal control of the rectilinear motion of a rigid body on a rough plane by means of the motion of two internal masses. J Appl Math Mech 72:126–135
36. Chernousko FL (2002) The optimum rectilinear motion of a two-mass system. J Appl Math Mech 66:1–7
37. Chernous'ko FL (2018) Optimal control of the motion of two-mass system. Dokl Akad Nauk 480:528–532
38. Bolotnik NN, Chernous'ko FL, Figurina T (2015) Optimal control of a two-body: vibration-driven locomotion system in a resistive environment. IFAC PapersOnLine 48:91–96
39. Gu X, Deng Z (2018) Dynamical analysis of vibro-impact capsule system with Hertzian contact model and random perturbation excitations. Nonlinear Dyn 92:1781–1789
40. LiuY PE, Wiercigroch M, Peng Z (2015) Forward and backward motion control of a vibro-impact capsule system. Int J Non-Linear Mech 70:30–46